ACS APPLIED MATERIALS & INTERFACES

Research Article

www.acsami.org

Widely Applicable Coinage Metal Window Electrodes on Flexible Polyester Substrates Applied to Organic Photovoltaics

Helena M. Stec and Ross A. Hatton*

Department of Chemistry, University of Warwick, Coventry CV4 7AL, United Kingdom

Supporting Information

ABSTRACT: The fabrication, exceptional properties, and application of 8 nm thick Cu, Ag, Au, and Cu/Ag bilayer electrodes on flexible polyethylene terephthalate (PET) and polyethylene naphthalate (PEN) substrates is reported. These electrodes are fabricated using a solvent free process in which the plastic surface is chemically modified with a molecular monolayer of thiol and amine terminated alkylsilanes prior to metal deposition. The resulting electrodes have a sheet resistance of ≤14 Ω sq^{-1}, are exceptionally robust and can be rapidly thermally annealed at 200 °C to reduce their sheet resistance to ≤9 Ω sq^{-1}. Notably, annealing Au electrodes briefly at 200 °C causes the surface to revert almost entirely to the {111} face, rendering it ideal as a model electrode for fundamental science and practical application alike. The power conversion efficiency of 1 cm^2 organic photovoltaics (OPVs) employing 8 nm Ag and Au films as the hole-extracting window electrode exhibit performance comparable to those on indium–tin oxide, with the advantage that they are resistant to repeated bending through a small radius of curvature and are chemically well-defined. OPVs employing Cu and bilayer Cu:Ag electrodes exhibit inferior performance due to a lower open-circuit voltage and fill factor. Measurements of the interfacial energetics made using the Kelvin probe technique provide insight into the physical reason for this difference. The results show how coinage metal electrodes offer a viable alternative to ITO on flexible substrates for OPVs and highlight the challenges associated with the use of Cu as an electrode material in this context.

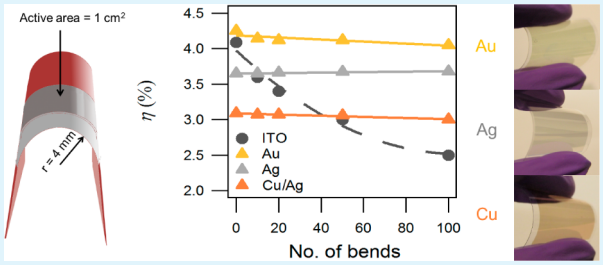

KEYWORDS: *electrode, polyethylene terephthalate, anneal, photovoltaic, solar cell, work function*

INTRODUCTION

Conducting oxides, such as indium–tin oxide (ITO) and fluorine-doped tin oxide (F:SnO_2) are almost universally employed as the transparent electrode in the current generation of organic photovoltaics (OPVs). However conducting oxide electrodes are not relevant for truly flexible OPVs because they are inherently brittle and so fail upon bending.[1,2] This limits their functionality and makes device fabrication using roll-to-roll processing methods problematic. Additionally, in order to achieve a sheet resistance <15 Ω sq^{-1}, oxide electrodes must be annealed at temperatures ≥300 °C,[3−6] a process that is incompatible with highly transparent flexible plastic substrates such as polyethylene naphthalate (PEN) and polyethylene terephthalate (PET). As a result the sheet resistance of commercially available ITO films supported on these plastics is typically >35 Ω sq^{-1}, which is 3−4 times higher than on glass.[6−8] Further drawbacks of conducting oxide electrodes are the high cost of patterning, the chemically ill-defined nature of the surface and the relatively high surface roughness. The latter two issues adversely impact the stability of the electrode contact with the adjacent semiconducting layer.[9−11] The complexity of ITO and other conducting oxides also makes it difficult to investigate the science of electrode−organic semiconductor contacts.[12] It is now widely recognized that the electrode interfaces are critical determinants of the performance of OPVs and that a great deal is yet to be understood about the process of charge carrier extraction in these devices.[13,14] As a result window electrodes that bridge the gap between model substrates required for fundamental science and truly flexible transparent electrodes for practical applications are highly desirable. In recent years a number of innovative flexible electrodes for OPVs have been proposed including printed metal grids,[15] carbon nanotube networks,[16,17] metal nanowires[18,19] and nanofibers,[20] graphene oxide[21] and graphene.[22] Readers are referred to reference 3 for a recent comprehensive review and critique of progress in these areas. Many of the aforementioned electrode technologies have the potential to realize the tantalizing prospect of wholly solution processed electrodes for OPV. However, all suffer from significant drawbacks which must be addressed if they are to replace conducting oxide electrodes. Rather surprisingly very few of the reports of alternative flexible electrodes for OPVs actually demonstrate device performance after repeated bending and most of those that do test devices with very small dimensions.[16,23,24a] As a result it is difficult to judge their suitability for use in flexible OPVs with cell areas greater than a few square millimeters.[25]

Received: August 16, 2012
Accepted: November 5, 2012
Published: November 5, 2012

   dx.doi.org/10.1021/am3016763 | ACS Appl. Mater. Interfaces 2012, 4, 6013−6020

The oldest category of window electrode is that of unpatterned thin metal films, which offer the advantages of simplicity, chemical homogeneity and established manufacturing infrastructure for large area roll-to-roll evaporation in the packaging industry.[26,27] The primary drawback of this class of transparent electrode is the reduced transparency across the visible and near-infrared spectrum as compared to optimized conducting oxide electrodes.[24] However, transparent electrodes based on thin metal films have been successfully employed in organic light-emitting diodes (OLEDs).[28−31] In the context of OPVs, optical modeling by O'Connor et al.[32] has shown that unpatterned sub-10 nm metal films have the potential to perform as well as conducting oxide coated glass due to microcavity light trapping effects. This has now been demonstrated in 4.4% efficient OPVs by Sergeant et al.,[33] who used 6 nm Ag electrodes sandwiched between thin MoO_x layers. More generally however, there are relatively few reports relating to the use of unpatterned metal films on flexible substrates as the transparent electrode for OPV.[24,34,35]

In addition to the negative perceptions about electrode transparency and sheet resistance a further reason why thin metal films on flexible substrates are not widely used as the transparent electrode in OPVs is that they can be extremely fragile.[3,20] To address this problem on rigid substrates such as glass and silicon, inorganic adhesive layer such as ZnS[36] or transition metal films can be used. Alternatively the substrate surface can be modified with a methoxysilane adhesive layer prior to metal deposition, although this approach is a relatively recent development and is not widely used.[28,37] Methoxysilanes form strong covalent bonds to the surface of glass by reaction with native hydroxyl groups and, unlike metal adhesion layers, do not contribute to light absorption by the electrode. This approach has been successfully employed for the fabrication of Au window electrodes on glass for OLEDs[28] and OPV[37] applications, although it has not to the best of our knowledge been used to prepare optically thin films of other coinage metals, nor has it been applied to plastic substrates. The reason for the latter is the absence of native surface groups onto which silanes can covalently bind on most technologically important plastics and the limitation imposed by the requirement for solvent orthogonality when chemically modifying plastics from solution.

Herein we report a method for the fabrication of 8 nm electrodes of Ag, Cu, Au, and Cu:Ag bilayer on PET and PEN using a molecular adhesive layer at the plastic surface. Using a Cu:Ag bilayer offers the possibility of simultaneously engineering the transparency of the electrode and lowering materials cost. A mixed molecular nanolayer of (3-aminopropyl)-trimethoxysilane (APTMS) and (3-mercaptopropyl)-trimethoxysilane (MPTMS) was chosen since nitrogen, present in APTMS, is known to coordinate with Cu,[38] Ag,[39] and Au[40] via its lone pair and the thiol moiety on MPTMS is known to bind to coinage metal surfaces via a strong covalent linkage.[41] The primary amine of APTMS also catalyzes the coupling reaction between methoxysilanes and alcohols,[42,43] speeding up the process of chemical derivatization. Au is selected because it is the electrode material of choice for the emerging fields of nanophotonics and advanced OLEDs[29,30] and is of wide applicability as a tool for fundamental scientific endeavor.[44] Ag and Cu are selected because they are the electrode metals of choice in OPV research due to their lower cost and higher electrical conductivity. For application in OPVs devices are typically annealed to 100−200 °C post-fabrication to realize optimal phase separation and/or crystallization of the organic semiconductor layer.[45,46] For this reason, the effect of annealing these electrodes at 200 °C is also reported. Finally the results of experiments designed to evaluate their suitability as a drop-in replacement for commercial ITO coated PET in flexible OPVs with a practical cell area of 1 cm^2 are reported.

METHODS

Preparation of Ultrathin Coinage Metal Films on PET and PEN. 100 μm PET-Hostaphan GN 4600 (Mitsubishi Polyester Film GmbH) and 125 μm thick PEN-Teonex (DuPont Teijin Films UK Ltd.) were cleaned by ultrasonic agitation for 15 min first in a dilute aqueous solution of Decon Neutracon then 2-propanol before UV/O_3 treatment (Novascan PSD-UVT). UV/O_3 treatment involved exposure of the substrates to UV light from a Hg lamp (185 and 254 nm, 20 mW/cm^2) at a distance of 25 mm from the substrate in an sealed air-filled chamber, followed by a 15 min incubation period. The substrates were immediately transferred to a desiccator where they were exposed to the vapor of APTMS:MPTMS at 50 mbar for 4 h before loading into an evaporator for Au deposition by thermal evaporation. The metal deposition rate was 0.1 nm s^{-1}. All metals were purchased from K.J. Lesker with 99.99% purity. The metal film thickness was measured using a carefully calibrated quartz-crystal microbalance mounted adjacent to the substrate. Substrates were annealed on a hot plate in a nitrogen atmosphere (<1 ppm O_2 and H_2O).

Sheet Resistance Measurement. Sheet resistance measurements were made using the 4-point probe Van der Pauw method on 26 mm × 26 mm substrates.

Optical Transparency Measurement. Far-field transparency measurements of the metal films were made over the wavelength range 400−750 nm using a Perkin-Elmer Lambda 25 UV Spectrometer. The incident light passed through the glass side first as is the case in an OPV. The reference material was either Hostaphan GN 4600 or Teonex depending on the electrode material.

Atomic Force Microscopy (AFM) Measurements of Surface Roughness. Tapping mode AFM and conductance measurements were performed in air using an Asylum Research MFP-3D. The surface roughness of substrates is quoted as the root-mean-square roughness (R_{rms}) measured over 5 × 5 μm^2 areas unless otherwise stated.

X-ray Diffraction (XRD). XRD measurements were carried out using a Siemens D5000 X-ray diffractometer operated in grazing angle or θ-2θ Bragg configuration using Cu (Kα) radiation. The voltage was set to 45 kV with a flux of 40 mA. Data for experiments were collected in the range from 30 to 120°, with a sampling interval of 0.05° and time per step of 4 s.

OPV Fabrication and Testing. ITO coated PET with a sheet resistance 45 Ω sq^{-1} was purchased from Sigma-Aldrich and cleaned in the same manner as PEN and PET substrates. Unless otherwise stated all chemicals were purchased from commercial sources and used without purification. Solution processed OPVs were fabricated according to the following procedure: A 10 nm MoO_x (Aldrich) film was evaporated under vacuum at 0.02 nm s^{-1}. PCDTBT (poly[N-9′-heptadecanyl-2,7-carbazole-alt-5,5-(4′,7′-di-2-thienyl-2′,1′,3′-benzothiadiazole)]) (Ossila) and $PC_{70}BM$ ([6,6]-phenyl-C_{70}-butyric acid methyl ester) (Ossila) were blended in a 1:3 ratio at a concentration 16 mg mL^{-1} in anhydrous chloroform. The blend was stirred for 1 h at 65 °C before filtering using a 0.45

μm polytetrafluoroethylene filter. PCDTBT:$PC_{70}BM$ bulk heterojunction films were prepared by spin-casting at 6000 r.p.m. for 60 s and annealing at 80 °C for 30 min. The electron-extracting electrode comprised an 8 nm bathocuproine (Aldrich) layer deposited at 0.05 − 0.10 nm s^{-1} followed by 100 nm of Al deposited through a shadow mask to give a device area of 1 cm^2. Small molecule OPVs were fabricated by depositing 1 nm PTCDA (Aldrich, 97%), purified once by thermal gradient sublimation and deposited at a rate of 0.01 nm s^{-1}. The molecular semiconductors pentacene (H. W. Sands Corp.) and C_{60} (Nano-C Inc., 99.5%) were deposited without prior purification at rates of 0.05 - 0.10 nm s^{-1} and 0.01 − 0.03 nm s^{-1} respectively to give 43 and 40 nm thickness respectively. The electron-extracting electrode comprised 8 nm bathocuproine layer deposited at 0.05−0.10 nm s^{-1} followed by 100 nm of Al deposited through a shadow mask to give a device area of 1 cm^2. *J*/*V* curves were measured in the dark and under 1 sun simulated solar illumination: 100 mW cm^{-2}; AM1.5G. The light intensity was calibrated using a PV Measurements Inc. calibrated silicon diode with KG5 color filter.

Bending Tests. Bending tests were conducted on 1 cm^2 OPVs. Devices were repeatedly bent through a radius of curvature of 4 mm.

High-Resolution X-ray Photoelectron Spectroscopy (HRXPS). XPS measurements were made using a Kratos Axis Ultra. Survey spectra in the range 1400−10 eV binding energy were recorded at an emission angle of 0° to the surface normal using an Al monochromated X-ray source operated at 15 kV and 5 mA emission. Each analysis area was approximately 700 × 300 μm^2. Analysis conditions were 160 eV pass energy, 1 eV steps, 0.2 s dwell per step and 1 scan. CasaXPS was used to measure the peak areas with the UK National Physical Laboratory (NPL) intensity calibration and commonly employed sensitivity factors to determine the concentrations of the detectable elements. The peak energies were corrected by referencing to the C 1s hydrocarbon peak at 285 eV and the spectra intensities corrected using a recent calibration using NPL's XPS Intensity Calibration Software. Two, three, or four components were used in the fits after a performing a linear background correction in CasaXPS.

Work Function Measurements (Kelvin Probe). All work function measurements were made in a nitrogen-filled glovebox using a Kelvin probe referenced to freshly cleaved highly oriented pyrolytic graphite (HOPG). Importantly the Kelvin probe is located adjacent to the vacuum evaporator in the same glovebox.

RESULTS AND DISCUSSION

Electrode Fabrication. PEN and PET are widely regarded as the substrates of choice for flexible organic optoelectronics due to their high transparency, good mechanical properties and resistance to oxygen and water vapor penetration.[15,47,48]The substitution of *p*-phenylene ring in PET with the bulkier naphthalene in PEN imparts a higher melting point[49] and increases absorption below 380 nm, thereby simultaneously improving thermal stability and filtering out UV photons which are suspected of degrading organic semiconductors.[50,51] The weak adhesion between coinage metal films deposited by vacuum evaporation and these plastics results in poor film quality. For example, Au films with an effective thickness of 8 nm on PET have a sheet resistance of 31 Ω sq^{-1}, which is a factor of 3 higher than that achieved using the method reported herein and is arguably too high for OPV applications. Furthermore upon 10 min ultrasonic agitation in water this increases 40 Ω sq^{-1}. When Cu films of the same thickness on PET are subject to an identical test they fail completely. The effect of brief ultrasonic agitation in various solvents on 8 nm Cu and Au films prepared by vacuum deposition directly onto PET and PEN substrates is summarized in Table S1 (see the Supporting Information). To improve the robustness of optically thin films of these metals on plastic substrates and promote uniform film growth at low thickness we have explored the possibility of chemically modifying the surface of PEN and PET substrates using a mixed monolayer of APTMS and MPTMS. Compatibility with flexible substrates is only possible because the monolayer is deposited from the vapor phase, which circumvents complexity that results from the frequent incompatibility of these plastics with solvents. Although APTMS and MPTMS couple to glass substrates via native surface hydroxyl groups, no such groups exist at the surface of PET or PEN and so it is necessary to introduce surface hydroxyl moieties without undermining the mechanical integrity of the surface. Oxidative treatments such as oxygen plasma[52] and UV/O_3[53] can be used to form reactive oxygen containing moieties at the surface of these plastics, although for the current purpose the latter method was found to be most suitable since it is less aggressive than plasma oxidation and does not increase the surface roughness (R_{rms}), which remained unchanged at 1.5 nm ±0.2 nm for treatment times of <5 min. The incorporation of hydrophilic moieties at the intrinsically hydrophobic polymer surface drastically alters its hydrophilicity and so the optimal oxidation time was determined by measuring the static water contact angle as a function of UV/O_3 treatment time. It is evident from Figure S1 (see the Supporting Information) that the increase in surface hydrophilicity begins to saturate after 4 min. This increase results from an increase in the density of oxygen containing moieties at the surface as verified using X-ray photoelectron spectroscopy (HRXPS) the results of which are summarized in Table S2 (see the Supporting Information). The proportion of the C 1s core level peak assigned to C−OH, −C−O-C- and COO-C increased by ∼3% on PET and ∼8% on PEN. To determine the optimal APTMS:MPTMS treatment time, we exposed PEN and PET substrates that were UV/O_3 treated for 4 min to the vapor of APTMS:MPTMS at a base pressure of ∼50 mbar for different times prior to evaporation of an 8 nm Au film. By measuring the ratio of the N 1s to S 2s peak areas in the high-resolution (HRXPS) spectra, and correcting for the instrument transmission function and average matrix sensitivity factor, the ratio of APTMS to MPTMS was determined to be 3.52 ± 1.1 on PET and 3.43 ± 0.03 on PEN.

It is evident from panels a and b in Figure 1 that the properties of Au films on PET and PEN are essentially identical. The same is true for Ag and Cu films fabricated on PET and PEN (Figure 1b), and so metal films on PET were used throughout the remainder of this study unless otherwise stated.

The roughness (R_{rms}) of 8 nm Au, Ag and Cu films fabricated on PET is very low (≤1.6 nm) and comparable to that of the underlying plastic (see the Supporting Information, Figure S2), consistent with the formation of a metal films of uniform thickness. Although the sheet resistance is 4−5 times higher than that calculated on the basis of the bulk resistivity of the metals,[54] because of scattering at the film surface and grain boundaries,[32] it is comparable to that of optimized ITO films on glass and thus low enough for use in OPVs.

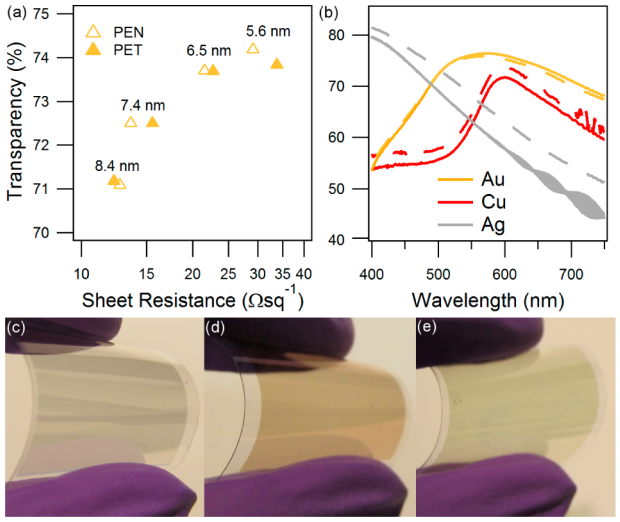

Figure 1. (a) Graph summarizing mean optical transparency over the range 400−750 nm as a function of sheet resistance for different thicknesses of Au on UV/O_3 treated PET and PEN derivatized with an APTMS:MPTMS nanolayer; (b) transparency spectra of 8 nm coinage metal films on nanolayer derivatized PET (continuous lines) and PEN (dashed lines); photographs of (c) Ag, (d) Cu, and (e) Au electrodes on nanolayer derivatized PET substrates.

The film robustness toward standard substrate cleaning procedures was tested by ultrasonic agitation in three common solvents; namely, 2-propanol, toluene, and water. Remarkably, these films were resistant to all of these solvent treatments with no significant change in sheet resistance (see the Supporting Information Table S3). For application as the substrate electrode in OPVs the properties of these electrodes must not deteriorate upon heating to 100−200 °C for short periods. Because of the low film thickness, the melting point of these metals is suppressed and so heating at 200 °C for only 10 min is sufficient to realize a 10−30% reduction in sheet resistance, depending on the metal, without significantly altering film topography (Table 1).

Table 1. Sheet Resistance of 8 nm Metal Electrodes on Derivatized PET before and after Annealing to 200 °C

	Au	Ag	Cu/Ag 6:2 Ω sq^{-1}	Cu/Ag 2:6	Cu
RT	12 ± 2	9 ± 2	14 ± 3	11 ± 2	11 ± 3
200 °C	9 ± 2	8 ± 2	11 ± 2	8 ± 2	8 ± 2

These films have a lower sheet resistance than most other unpatterned metal films of the same thickness on glass and plastic substrates reported to date.[31,32,36,55a−e] The notable exception is the 6 nm Ag films sandwiched between MoO_x layers reported by Sergeant et al.,[33] who achieved 6.2 Ω sq^{-1} by evaporating Ag onto MoO_x coated glass substrates held at −5 °C, although MoO_x/Ag/MoO_x films fabricated in our laboratory were not robust toward ultrasonic agitation. The reduction in sheet resistance upon annealing is attributed to an increase in film crystallinity which reduces the number of grain boundaries and defects at which electrons are scattered, since it is known that annealing much thicker Au films on glass increases the crystal grain size.[44,56] Importantly, annealing reduces the sheet resistance of all the single component films and the Cu (2 nm):Ag (6 nm) bilayer films to ≤9 Ω sq^{-1}, which represents a significant further improvement.

Wanunu et al. have previously reported highly crystalline 15 nm Au films on glass with a mean transparency across the visible spectrum of 32% and demonstrated application as a versatile, chemically well-defined substrate for surface science.[44] Because the Au films fabricated here offer the advantage of; (i) flexibility; (ii) more than twice the far-field transparency; (iii) and half the Au usage, the possibility of achieving the high degree of crystallinity reported by Wanunu et al. in a much shorter time frame was investigated. Au films with thicknesses in the range 5.6−8.4 nm were annealed up to 200 °C for 10 min.

It is evident from Figure 2a that the largest percentage reduction in sheet resistance upon brief thermal annealing at

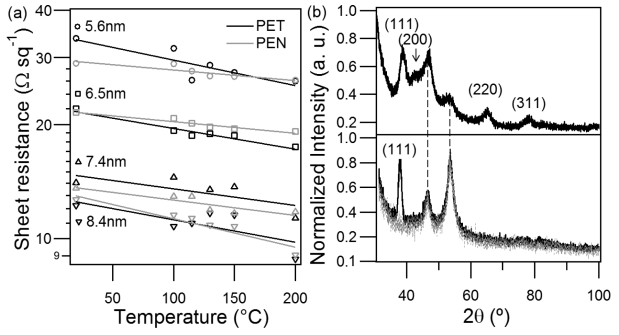

Figure 2. (a) Graph showing changes in sheet resistance with annealing temperature for different Au film thickness; (b) (upper) Grazing incidence XRD spectrum of an 8.4 nm Au film supported on APTMS:MPTMS derivatized PET; (lower) θ−2θ XRD spectra of PET (gray) and 8.4 nm Au film supported on APTMS:MPTMS derivatized PET (black) after annealed at 200 °C for 10 min.

200 °C is achieved for the thickest Au films: 8.4 nm, which exhibit a 25% decrease from 12.5 Ω sq^{-1} to 9 Ω sq^{-1} without any significant change in R_{rms} (1.5 nm ± 0.2 nm vs 1.3 nm ± 0.1 nm) or transparency. Grazing angle XRD spectra of Au films on PET prior to annealing show weak reflections from the Au {111}, {200}, {220} and {311} crystal planes (Figure 2b). Upon annealing at 200 °C for 10 min, an intense Au {111} reflection emerges such that it is no longer necessary to record the spectrum at grazing angle. This dramatic change is direct evidence that the surface reverts almost entirely to the {111} crystallographic face rendering these electrodes both chemically and structurally well-defined. This transformation is remarkable in that it occurs so rapidly and renders these electrodes near perfect for organic optoelectronics, bridging the gap between model substrates required for fundamental science and truly flexible window electrodes for applications. This study also corroborates the earlier conclusion that the reduction in the sheet resistance of these metal films upon annealing results from an increase in the degree of film crystallinity.

It is evident from Figure 1b that the far-field transparency of the Ag, Cu and Au films is significantly different, with Au films offering the highest transparency (71% (Au) vs 61% (Ag) and 62% (Cu)) and broadest band transparency across the visible spectrum. Ag and Cu films are most transparent at opposite ends of the visible spectrum, so to realize an electrode with broad band transparency at a lower materials cost than Au, bilayer Ag and Cu were fabricated with the Cu layer buried beneath the Ag layer to protect it against oxidation. It is evident from Figure 3a that this approach works best for 1:1 Cu:Ag films: although the mean transparency of Cu (4 nm): Ag (4

dx.doi.org/10.1021/am3016763 | ACS Appl. Mater. Interfaces 2012, 4, 6013−6020

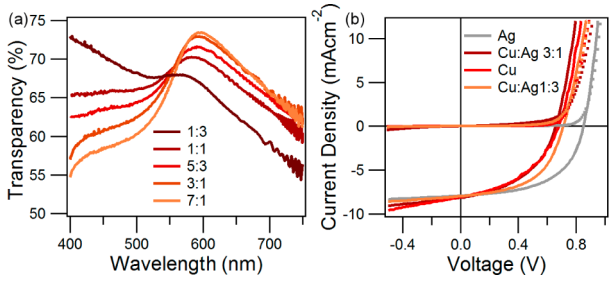

Figure 3. (a) Transparency spectra of 8 nm Cu:Ag bilayer films with different Cu:Ag ratios supported on APTMS:MPTMS derivatized PET; (b) *J*/*V* characteristics of devices in the dark (dotted lines) and under 1 sun simulated solar illumination (solid lines) with the structure: 8 nm metal electrode on APTMS:MPTMS derivatized PET/10 nm MoO_x/PCDTBT:$PC_{70}BM$/8 nm bathocuproine/100 nm Al.

nm) films (65%) is 7% lower than Au electrodes of the same thickness, it is higher than that of the pure Ag (61%) or Cu (62%) films of the same thickness with a broader band transparency.

Device Fabrication and Testing. To demonstrate the viability of these electrodes as a drop-in replacement for ITO in flexible OPVs they were incorporated into solution processed OPVs with the structure: hole-extracting electrode/MoO_x (10 nm)/(PCDTBT:$PC_{70}BM$) bulk-heterojunction (60 nm)/bathocuproine (8 nm)/Al. In this device structure, the bathocuproine layer serves as an exciton blocking layer at the contact with the electron extracting electrode. MoO_x is a widely used hole-extraction material for OPVs and is doped *n*-type by gap states resulting from partial filling of unoccupied 4d orbitals of Mo atoms neighboring oxygen vacancies.[57] Its functionality stems from its exceptionally high work function[58] which results in spontaneous ground-state charge transfer from the highest occupied molecular orbital (HOMO) of the organic semiconductor and the Fermi level (E_f) of the electrode which pins these energy levels close to one another on either side of the oxide layer.[57,59] Charge transport across the oxide layer is mediated either by the gap states themselves[57] or via electron transport in the conduction band[59] depending on the degree of n-type doping. PCDTBT:$PC_{70}BM$ is a bulk-heterojunction material system capable of achieving $\eta > 5\%$ in small area ($\ll 1$ cm^2) device architectures.[60,61] This material system harvests light across almost the entire visible spectrum and so is ideally suited to investigate the applicability of window electrodes with a strongly wavelength dependent transparency across the visible spectrum.

To a first approximation the short circuit current (J_{sc}) in 1 cm^2 OPVs scales with the electrode transparency: Ag (T = 61%, J_{sc} = 7.7 ± 0.1 mA cm^2); Cu (T = 62%, J_{sc} = 8.1 ± 0.1 mA cm^2); Au (T = 71%, J_{sc} = 8.45 ± 0.15 mA cm^2); ITO (T = 81%, J_{sc} = 9.60 ± 0.40 mA cm^2). The difference in J_{sc} between devices employing Ag and Cu electrodes, as compared to Au, is smaller than expected on the basis of transparency alone. This is attributed to microcavity effects,[33] because both Cu and Ag have a higher reflectivity than Au across the visible spectrum.[62] Crucially the η of OPVs fabricated on Ag and Au electrodes, 3.7% ± 0.15 and 4.25% ± 0.2, respectively, is comparable to that of devices using ITO electrodes, 4.10% ± 0.15, due to the higher fill factors (FF); (Ag) 0.55 ± 0.03, (Au) 0.60 ± 0.01, and (ITO) 45 ± 0.03. The origin of this improvement is the lower cell series resistance, which is evident from the gradient of the *J*/*V* characteristic at J = 0 and results from the lower sheet resistance of the metal electrodes (9–12 Ω sq^{-1}) as compared to ITO (45 Ω sq^{-1}) on PET. To demonstrate the generality of this result, wholly vacuum deposited 1 cm^2 OPVs based on a pentacene/C_{60} heterojunction were also fabricated on Au and ITO electrodes on PET and PEN. Au electrodes were used since they exhibit the best performance of the metal electrodes in solution processed OPVs. Again, device performance on Au electrodes exceeds that on ITO coated PET (0.85% ± 0.03% vs 0.64% ± 0.07%) due to the higher FF (0.46 ± 0.01 vs 0.31 ± 0.03). Notably, because these electrodes are fabricated using vacuum evaporation their fabrication can be seamlessly integrated with that of wholly evaporated molecular photovoltaics. Details of these experiments are provided in the Supporting Information (Figure S3 and Table S4).

It is evident from Figure 4a that the performance of OPVs on Cu electrodes is inferior to that on Ag and Au due to the lower

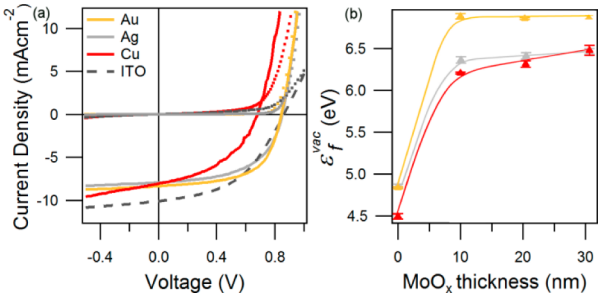

Figure 4. (a) *J*/*V* characteristics of devices in the dark (dotted lines) and under 1 sun simulated solar illumination (solid lines) with structure: 8 nm metal electrode on APTMS:MPTMS derivatized PET/10 nm MoO_x/PCDTBT:$PC_{70}BM$/8 nm bathocuproine/100 nm Al.; (b) The variation in ε_f^{vac} across MoO_x layers deposited onto Au, Ag, and Cu electrodes as function of MoO_x thickness.

V_{oc} and *FF*. The latter results from a lower shunt resistance as is evident from the steeper gradient of the *J*/*V* characteristic at V = 0. The reason for the lower V_{oc} is the earlier onset of dark current injection under forward bias which is indicative of a smaller built-in potential. Interestingly this correlates with the work function of the electrodes measured immediately prior to device fabrication using a Kelvin probe; Cu: 4.52 ± 0.03 eV; Ag: 4.87 ± 0.01 eV; Au: 4.85 ± 0.01 eV, since the work function of the Cu electrode is 0.25–0.30 eV lower than the Ag or Au electrodes. However, this simplistic explanation does not take account of the important role played by the MoO_x layer, which should align the E_f of the electrode close to the HOMO in PCDTBT so that the difference in work function between these electrodes does not translate to a difference in built-in potential.

To gain further insight into the interfacial energetics, measurements of the change in energy between the electrode E_f and the vacuum level at the surface (VL_s) were made as a function of MoO_x layer thickness using a Kelvin probe (see Figure 4b). This energy difference, ε_f^{vac}, corresponds to the work function of the oxide when the film thickness is sufficient for E_f alignment to be established across the interface.[63] If thermodynamic equilibrium is not achieved then ε_f^{vac} corresponds to the work function of the metal electrode with a modified surface potential.[14,63] This technique has been used extensively to probe interfacial energetics at electrode–organic semiconductor interfaces and has the advantage over photoelectron spectroscopy that it can be used to investigate the

dx.doi.org/10.1021/am3016763 | ACS Appl. Mater. Interfaces 2012, 4, 6013–6020

change in potential across relatively thick films of wide band gap materials.[14,63] To the best of the authors' knowledge, this is the first time that a comparative study of the energetics at the interface between MoO_x and Cu, Ag, and Au electrodes, or the correlation with OPV device performance has been reported.

For the thickness of MoO_x used in devices (10 nm) the change in ε_f^{vac} is different on all three substrates indicting that E_f alignment is not achieved across at least two of the three interfaces. In those cases, the thin oxide layer simply modifies the surface potential of the substrate electrode such that it has a work function much greater than the ionization potential (I_p) of PCDTBT (5.35 eV).[64] Because ε_f^{vac} on the Au electrode exhibits the largest change and remains constant with increasing layer thickness at a value equal to the work function of MoO_x reported in the literature; 6.9 eV,[57,59] it is likely that thermodynamic equilibrium has been achieved across this interface. This result is in excellent agreement with measurements of the interfacial energetics between Au substrates and MoO_x by Seki et al.[57] using photoelectron spectroscopy. Under these circumstances E_f of the Au electrode is aligned closely to the HOMO of PCDTBT, which ensures that the built-in electric field in the diode is maximized. As a result the onset of hole-injection under forward bias is delayed as much as possible, ensuring that V_{oc} is maximized. By extension, at the interface between the 10 nm MoO_x layer and Ag and Cu electrodes there is suboptimal energy level alignment. Since it is reasonable to assume that the HOMO of PCDTBT is always pinned to the E_f of the MoO_x[58] the performance of OPVs employing both Ag and Cu electrodes should be inferior to that achieved using Au electrodes due to the smaller built-in potential, which results in an earlier onset of dark current injection. Although it is clear from Figure 4a that this is the case for the Cu electrode it does not hold true for the Ag electrode. The measurements of the energetics at the metal electrode/MoO_x interface cannot therefore be rationalized in terms of a well-defined interface. Instead, it is necessary to account for the possibility that Ag and Cu diffuse into the thin MoO_x overlayer.[35,65] Indeed, the very low thickness of these metal films suppresses the temperature at which metal diffusion occurs, which is why these films are amenable to rapid annealing at 200 °C. Ag is known to diffuse less aggressively into oxide overlayers[65] and so it is plausible that those Ag atoms that do diffuse into the MoO_x function as *n*-type dopants, much like Mo atoms, moving the Fermi level closer to the conduction band edge and thus reducing the work function of the oxide. This hypothesis offers an explanation as to why ε_f^{vac} at the Ag/MoO_x interface converges to a lower work function than MoO_x on Au. It also offers a plausible explanation as to why OPVs employing a Ag electrode have the same V_{oc} as those using a Au electrode, since the work function of Ag doped MoO_x (~6.4 eV, from Figure 4b) is still sufficiently high to align the electrode E_f (~4.9 eV below VL_s) with the HOMO of PCDTBT (5.35 eV below VL_s).[64] Conversely Cu is known to diffuse very aggressively into metal oxides including MoO_x,[35] and so it is possible that filamentary strands of metallic Cu extend along the grain boundaries all the way through the 10 nm MoO_x layer, thereby undermining it electronic functionality. This would explain why ε_f^{vac} does not saturate with increasing MoO_x thickness, but continues to increase toward that of MoO_x on Au. It would also explain the early onset of dark current injection under forward bias, since the work function of Cu is too low for the E_f of the electrode to align closely with the HOMO in PCDTBT. The deterioration in FF can also be rationalized in terms of this hypothesis because the role of the oxide layer in reducing filamentary short circuits is undermined.[66,67]

To explore the potential of tuning the optical properties of these metal film electrodes bilayer Cu:Ag electrodes were fabricated with different relative thicknesses. In principle, these electrodes also offered a path to circumventing the aforementioned problem with Cu electrodes, because the Ag forms the interface with the MoO_x hole-extraction layer. The total metal thickness was kept at 8 nm and the bilayer Cu:Ag thickness ratio was 1:0, 3:1, 1:3, and 0:1. It is clear from the *J*/*V* characteristics that when the Ag layer thickness is 2 nm the electrode essentially behaves as if it were Cu only. Increasing the Ag thickness to 6 nm results in a relatively small improvement in both V_{oc} and *FF*, which is well short of that achieved on Ag alone (Figure 3b). Pitts et al.[68] have shown that Cu can diffuse at room temperature through Ag overlayers as thick as 11 nm and so these results can also be rationalized in terms of the diffusion of Cu into the MoO_x layer and highlights the challenges associated with the using Cu electrodes in OPV.

Finally, it is widely considered that for OPVs to realize their full commercial potential they must be fabricated on flexible substrates. Panels a and b Figure 5 show how the efficiency of 1

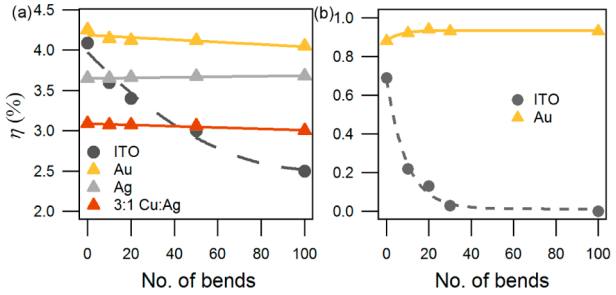

Figure 5. Power conversion efficiency as a function of number of bend cycles for; (a) PCDTBT:$PC_{70}BM$-based OPV with Au/PET (yellow triangles), Cu/PET (brown triangles), Ag/PET (gray triangles), or ITO/PET (closed circle) as the substrate window electrode; (b) C_{60}/pentacene-based OPV with Au/PET (yellow triangles) and ITO/PET (closed circles) electrodes.

cm^2 solution processed and small molecule OPVs fabricated on ITO and metal electrodes on PET perform as a function of the number of bend cycles through a radius of curvature of 4 mm. The performance of devices with an ITO electrode deteriorates rapidly. In contrast, the performance of both solution-processed and vacuum-deposited OPVs with metal electrodes is practically unchanged even after 100 bend cycles, opening the door to the realization of truly flexible OPVs.

CONCLUSIONS

In summary, 8 nm thick Cu, Ag, Au and bilayer Cu/Ag films have been fabricated on the technologically important plastic substrates PET and PEN chemically modified with a mixed molecular adhesive layer to realize highly electrically conductive, low surface roughness, and exceptionally robust window electrodes. Because of their low thickness, these films are amenable to rapid annealing at only 200 °C to reduce the sheet resistance to $\leq 9\ \Omega\ sq^{-1}$. To the best of the authors' knowledge, the properties of these electrodes in terms of robustness and sheet resistance are superior to almost all unpatterned metal film electrodes of the same thickness on plastic substrates reported to date. The results of OPV device

studies, combined with measurements of the interfacial energetics, show that these electrodes offer a viable alternative to ITO on flexible substrates for practical application and highlight the complexity associated with the use of Cu as an electrode material in this context.

■ ASSOCIATED CONTENT

Supporting Information

Table S1, sheet resistance of 8 nm Au and Cu films supported on untreated PEN and PET substrates before and after ultrasonic agitation in three common solvents: toluene, water and 2-propanol; Figure S1, static water contact angle on PEN and PET substrates as a function of UV/O_3 treatment time; Table S2, C 1s and O 1s HRXPS survey scan summaries before and after UV/O_3 treatment of PET and PEN expressed as atomic percentages and proportion of C 1s peak assigned to C−OH, −C−O−C−, and COO−C bonding environments; Figure S2, representative AFM images of 8 nm metal films supported on APTMS:MPTMS derivatized PET; Table S3, sheet resistance of 8 nm metal films supported on PEN and PET substrates derivatized with an APTMS:MPTMS nanolayer before and after ultrasonic agitation in three common solvents: toluene, water, and 2-propanol.; Figure S3, *J*/*V* characteristics of devices in the dark and under 1 sun simulated solar illumination with the structure: 8.4 nm Au on APTMS: MPTMS derivatized PET or PEN (or ITO PET)/1 nm PTCDA/43 nm pentacene/40 nm C_{60}/8 nm bathocuproine/ 100 nm Al; Table 4S, summary of the key device performance characteristics for OPVs with a device structure: electrode (8.4 nm Au or ITO)/PTCDA/pentacene/C_{60}/BCP/Al. This material is available free of charge via the Internet at http://pubs.acs.org/.

■ AUTHOR INFORMATION

Corresponding Author

*Tel.: + 44 (0)24761 50874. E-mail: ross.hatton@warwick.ac.uk.

Author Contributions

The manuscript was written through contributions of all authors. All authors have given approval to the final version of the manuscript.

Notes

The authors declare no competing financial interest.

■ ACKNOWLEDGMENTS

This work was supported by the UK Engineering and Physical Sciences Research Council (EPSRC) and the European Regional Development Agency/Advantage West Midlands Science City Materials Initiative (Project 2). R.A.H. is grateful to the Royal Academy of Engineering/EPSRC for the award of a Fellowship. We thank Mr. Steve Spencer and Dr. Alex Shard (National Physical Laboratory) for assistance with the XPS data collection and analysis. The PET and PEN substrates were provided courtesy of Mitsubishi Polyester Film GMBH and DuPont Teijin Films UK Ltd, respectively.

■ REFERENCES

(1) Cairns, D. R.; Witte, R. P.; Sparacin, D. K.; Sachsman, S. M.; Paine, D. C.; Crawford, G. P.; Newton, R. R. *Appl. Phys. Lett.* **2000**, *76*, 1425−1427.
(2) Cairns, D. R.; Crawford, G. P. *Proc. IEEE* **2005**, *93*, 1451−1458.
(3) Hecht, D. S.; Hu, L. B.; Irvin, G. *Adv. Mater.* **2011**, *23*, 1482−1513.
(4) Jeong, W. I.; Lee, J.; Park, S. Y.; Kang, J. W.; Kim, J. J. *Adv. Funct. Mater.* **2011**, *21*, 343−347.
(5) Fortunato, E.; Ginley, D.; Hosono, H.; Paine, D. C. *MRS Bull.* **2007**, *32*, 242−247.
(6) Song, S.; Yang, T.; Liu, J.; Xin, Y.; Li, Y.; Han, S. *Appl. Surf. Sci.* **2011**, *257*, 7061−7064.
(7) Choi, K. H.; Jeong, J. A.; Kang, J. W.; Kim, D. G.; Kim, J. K.; Na, S. I.; Kim, D. Y.; Kim, S. S.; Kim, H. K. *Sol. Energy. Mater. Sol. Cells* **2009**, *93*, 1248−1255.
(8) Hamasha, M. M.; Dhakal, T.; Alzoubi, K.; Albahri, S.; Qasaimeh, A.; Lu, S. S.; Westgate, C. R. *J. Disp. Technol.* **2012**, *8*, 383−388.
(9) Armstrong, N. R.; Veneman, P. A.; Ratcliff, E.; Placencia, D.; Brumbach, M. *Acc. Chem. Res.* **2009**, *42*, 1748−1757.
(10) Jonda, C.; Mayer, A. B. R.; Stolz, U.; Elschner, A.; Karbach, A. *J. Mater. Sci.* **2000**, *35*, 5645−5651.
(11) Yambem, S. D.; Liao, K. S.; Alley, N. J.; Curran, S. A. *J. Mater. Chem.* **2012**, *22*, 6894−6898.
(12) Pegg, L. J.; Hatton, R. A. *ACS Nano* **2012**, *6*, 4722−4730.
(13) Chen, L. M.; Xu, Z.; Hong, Z. R.; Yang, Y. *J. Mater. Chem.* **2010**, *20*, 10947.
(14) Cook, R. M.; Pegg, L.-J.; Kinnear, S. L.; Hutter, O. S.; Morris, R. J. H.; Hatton, R. A. *Adv. Energy Mater.* **2011**, *1*, 440−447.
(15) Galagan, Y.; Rubingh, J.; Andriessen, R.; Fan, C. C.; Blom, P. W. M.; Veenstra, S. C.; Kroon, J. M. *Sol. Energy Mater. Sol. Cells* **2011**, *95*, 1339−1343.
(16) Rowell, M. W.; Topinka, M. A.; McGehee, M. D.; Prall, H. J.; Dennler, G.; Sariciftci, N. S.; Hu, L. B.; Gruner, G. *Appl. Phys. Lett.* **2006**, *88*, 233506.
(17) Zhang, D.; Ryu, K.; Liu, X.; Polikarpov, E.; Ly, J.; Tompson, M. E.; Zhou, C. *Nano Lett.* **2006**, *6*, 1880−1886.
(18) Kang, M. G.; Park, H. J.; Ahn, S. H.; Guo, L. J. *Sol. Energy Mater. Sol. Cells* **2010**, *94*, 1179−1184.
(19) De, S.; Higgins, T. M.; Lyons, P. E.; Doherty, E. M.; Nirmalraj, P. N.; Blau, W. J.; Boland, J. J.; Coleman, J. N. *ACS Nano* **2009**, *3*, 1767−1774.
(20) Wu, H.; Hu, L. B.; Rowell, M. W.; Kong, D. S.; Cha, J. J.; McDonough, J. R.; Zhu, J.; Yang, Y. A.; McGehee, M. D.; Cui, Y. *Nano Lett.* **2010**, *10*, 4242−4248.
(21) Eda, G.; Fanchini, G.; Chhowalla, M. *Nat. Nanotechnol.* **2008**, *3*, 270−274.
(22) Li, X.; Zhu, Y.; Cai, W.; Borysiak, M.; Han, B.; Chen, D.; Piner, R. D.; Colombo, L.; Ruoff, R. S. *Nano Lett.* **2009**, *9*, 4359−4363.
(23) Hau, S. K.; Yip, H. L.; Zou, J. Y.; Jen, A. K. Y. *Org. Electron.* **2009**, *10*, 1401−1407.
(24) (a) Yambem, S. D.; Liao, K. S.; Curran, S. A. *Sol. Energy Mater. Sol. Cells* **2011**, *95*, 3060−3064. (b) Yambem, S. D.; Haldar, A.; Liao, K.-S.; Dillon, E. P.; Barron, A. R.; Curran, S. A. *Sol. Energy Mater. Sol. Cells* **2011**, *95*, 2424−2430.
(25) Hu, L.; Wu, H.; Cui, Y. *MRS Bull.* **2011**, *36*, 760−765.
(26) Klauk, H. *Organic Electronics*; Wiley-VCH: Weinheim, Germany, 2008.
(27) Lange, J.; Wyser, Y. *Packag. Technol. Sci.* **2003**, *16*, 149−158.
(28) Hatton, R. A.; Willis, M. R.; Chesters, M. A.; Briggs, D. *J. Mater. Chem.* **2003**, *13*, 722−726.
(29) Helander, M. G.; Wang, Z. B.; Greiner, M. T.; Liu, Z. W.; Qiu, J.; Lu, Z. H. *Adv. Mater.* **2010**, *22*, 2037−2040.
(30) Wang, Z. B.; Helander, M. G.; Qiu, J.; Puzzo, D. P.; Greiner, M. T.; Hudson, Z. M.; Wang, S.; Liu, Z. W.; Lu, Z. H. *Nat. Photonics* **2011**, *5*, 753−757.
(31) Hong, K.; Kim, K.; Kim, S.; Lee, I.; Cho, H.; Yoo, S.; Choi, H. W.; Lee, N. Y.; Tak, Y. H.; Lee, J. L. *J. Phys. Chem. C* **2011**, *115*, 3453−3453.
(32) O' Connor, B.; Haughn, C.; An, K. H.; Pipe, K. P.; Shtein, M. *Appl. Phys. Lett.* **2008**, *93*, 223304.
(33) Sergeant, N. P.; Hadipour, A.; Niesen, B.; Cheyns, D.; Heremans, P.; Peumans, P.; Rand, B. P. *Adv. Mater.* **2012**, *24*, 728−732.

(34) Kim, J. B.; Kim, P.; Pegard, N. C.; Oh, S. J.; Kagan, C. R.; Fleischer, J. W.; Stone, H. A.; Loo, Y. L. *Nat. Photonics* **2012**, *6*, 327−332.
(35) Perez Lopez, I.; Cattin, L.; Nguyen, D.-T.; Morsli, M.; Bernede, J. C. *Thin Solid Films* **2012**, *520*, 6419−6419.
(36) Lim, S; Han, D.; Kim, H.; Lee, S.; Yoo, S. *Sol. Energy Mater. Sol. Cells* **2012**, *101*, 170−175.
(37) Stec, H. M.; Williams, R. J.; Jones, T. S.; Hatton, R. A. *Adv. Funct. Mater.* **2011**, *21*, 1709−1716.
(38) Karlin, K. D.; Dahlstrom, P. L.; Hyde, J. R.; Zubieta, J. *J. Chem. Soc., Chem. Commun.* **1980**, 906−908.
(39) Pickering, A. L.; Long, D. L.; Cronin, L. *Inorg. Chem.* **2004**, *43*, 4953−4961.
(40) Hoft, R. C.; Ford, M. J.; McDonagh, A. M.; Cortie, M. B. *J. Phys. Chem. C* **2007**, *111*, 13886−13891.
(41) Laibinis, P. E.; Whitesides, G. M.; Allara, D. L.; Tao, Y. T.; Parikh, A. N.; Nuzzo, R. G. *J. Am. Chem. Soc.* **1991**, *113*, 7152−7167.
(42) Vrancken, K. C.; Possemiers, K.; Vandervoort, P.; Vansant, E. F. *Colloids Surf., A 98*, 235-241.
(43) Kallury, K. M. R.; Macdonald, P. M.; Thompson, M. *Langmuir* **1994**, *10*, 492−499.
(44) Wanunu, M.; Vaskevich, A.; Rubinstein, I. *J. Am. Chem. Soc.* **2004**, *126*, 5569−5576.
(45) Moon, J. S.; Takacs, C. J.; Sun, Y. M.; Heeger, A. J. *Nano Lett.* **2011**, *11*, 1036−1039.
(46) Wei, G. D.; Lunt, R. R.; Sun, K.; Wang, S. Y.; Thompson, M. E.; Forrest, S. R. *Nano Lett.* **2010**, *10*, 3555−3559.
(47) Ito, S.; Ha, N. L. C.; Rothenberger, G.; Liska, P.; Comte, P.; Zakeeruddin, S. M.; Pechy, P.; Nazeeruddin, M. K.; Gratzel, M. *Chem. Commun.* **2006**, 4004−4006.
(48) Logothetidis, S.; Laskarakis, A.; Georgiou, D.; Amberg-Schwab, S.; Weber, U.; Noller, K.; Schmidt, M.; Kuecuekpinar-Niarchos, E.; Lohwasser, W. *Eur. Phys. J.−Appl. Phys.* **2010**, *51*, 33203.
(49) Karacan, I. *J. Appl. Polym. Sci.* **2006**, *100*, 142−160.
(50) Jorgensen, M.; Norrman, K.; Krebs, F. C. *Sol. Energy Mater. Sol. Cells* **2008**, *92*, 686−714.
(51) Sullivan, P.; Jones, T. S. *Org. Electron.* **2008**, *9*, 656−660.
(52) Nakamura, Y.; Suzuki, Y.; Watanabe, Y. *Thin Solid Films* **1996**, *291*, 367−369.
(53) Ozcam, A. E.; Efimenko, K.; Jaye, C.; Spontak, R. J.; Fischer, D. A.; Genzer, J. *J. Electron Spectrosc.* **2009**, *172*, 95−103.
(54) Schakelford, J. F. *Introduction to Material Science for Engineers*; MacMillan: New York, 1992.
(55) (a) Cho, H.; Yun, C.; Park, J.-W.; Yoo, S. *Org. Electron.* **2009**, *10*, 1163−1169. (b) Ghosh, D. S.; Chen, T. L.; Pruneri, V. *Appl. Phys. Lett.* **2010**, *96*, 091106−3. (c) Jung, G. H.; Hong, K.; Dong, W. J.; Kim, S.; Lee, J.-L. *Adv. Energy Mater.* **2011**, *1*, 1023−1028. (d) Wilken, S.; Hoffmann, T.; von Hauff, E.; Borchert, H.; Parisi, J. *Sol. Energy Mater. Sol. Cells* **2012**, *96*, 141−147. (e) Zhang, M.; Chiu, T.-L.; Lin, C.-F.; Lee, J.-H.; Wang, J.-K.; Wu, Y. *Sol. Energ. Mater. Sol. Cells* **2011**, *95*, 2606−2609.
(56) Golan, Y.; Margulis, L.; Rubinstein, I. *Surf. Sci.* **1992**, *264*, 312−326.
(57) Kanai, K.; Koizumi, K.; Ouchi, S.; Tsukamoto, Y.; Sakanoue, K.; Ouchi, Y.; Seki, K. *Org. Electron.* **2010**, *11*, 188−194.
(58) Greiner, M. T.; Helander, M. G.; Tang, W. M.; Wang, Z. B.; Qiu, J.; Lu, Z. H. *Nat. Mater.* **2012**, *11*, 76−81.
(59) Kroeger, M.; Hamwi, S.; Meyer, J.; Riedl, T.; Kowalsky, W.; Kahn, A. *Appl. Phys. Lett.* **2009**, *95*, 123301.
(60) Alem, S.; Chu, T.-Y.; Tse, S. C.; Wakim, S.; Lu, J.; Movileanu, R.; Tao, Y.; Belanger, F.; Desilets, D.; Beaupre, S.; Leclerc, M.; Rodman, S.; Waller, D.; Gaudiana, R. *Org. Electron.* **2011**, *12*, 1788−1793.
(61) Manor, A.; Katz, E. A.; Tromholt, T.; Hirsch, B.; Krebs, F. C. *Appl. Phys. Lett.* **2011**, *109*, 074508−9.
(62) Rohsenow, W. M., Choi, H. *Heat Mass and Momentum Transfer*; Prentice Hall: New York, 1961.
(63) Ishii, H.; Sugiyama, K.; Ito, E.; Seki, K. *Adv. Mater.* **1999**, *11*, 605−625.
(64) Watters, D. C.; Kingsley, J.; Yi, H. N.; Wang, T.; Iraqi, A.; Lidzey, D. *Org. Electron.* **2012**, *13*, 1401−1408.
(65) Winkler, T.; Schmidt, H.; Flugge, H.; Nikolayzik, F.; Baumann, I.; Schmale, S.; Weimann, T.; Hinze, P.; Johannes, H. H.; Rabe, T.; Hamwi, S.; Riedl, T.; Kowalsky, W. *Org. Electron.* **2011**, *12*, 1612−1618.
(66) Dahou, F. Z.; Cattin, L.; Garnier, J.; Ouerfelli, J.; Morsli, M.; Louarn, G.; Bouteville, A.; Khellil, A.; Bernede, J. C. *Thin Solid Films* **2010**, *518*, 6117−6122.
(67) Varnamkhasti, M. G.; Fallah, H. R.; Mostajaboddavati, M.; Ghasemi, R.; Hassanzadeh, A. *Sol. Energy Mater. Sol. Cells* **2012**, *98*, 379−384.
(68) Pitts, J. R.; Czanderna, A. W.; Thomas, T. M. *J. Vac. Sci. Technol. A* **1986**, *4*, 1671−1674.